

Coexistence of room-temperature negative differential resistance and unsaturated magnetoresistance effects in germanium-based devices

Xiong He(何雄), Ling Cai(蔡玲), Li-Zhi Yi(易立志), Guang-Duo Lu(鲁广铎), Li-Qing Pan(潘礼庆), and Zhi-Gang Sun(孙志刚)

Citation: Chin. Phys. B, 2026, 35 (**3**): 037502. DOI: 10.1088/1674-1056/adfdc3
http://cpb.iphy.ac.cn; http://iopscience.iop.org/cpb

What follows is a list of articles you may be interested in

Anomalous Hall effect and Lifshitz transition in Fe_3Sn_2 nanosheets

Xue Yang(杨雪), Jijian Liu(刘继健), Xinyi Zheng(郑新义), Lei Xu(徐磊), Lihong Hu(胡利洪), Sicheng Zhou(周思成), Siyuan Zhou(周思远), Ximing Zhang(张栖铭), Bingbing Tong(仝冰冰), Jie Shen(沈洁), Zhaozheng Lyu(吕昭征), Xiunian Jing(景秀年), Fanming Qu(屈凡明), Peiling Li(李沛岭), Jiadong Zhou(周家东), Guangtong Liu(刘广同), and Li Lü(吕力)

Chin. Phys. B, 2026, 35 (**1**): 017503. DOI: 10.1088/1674-1056/ae101b

Temperature-dependent magnetotransport properties of $CoFe_2O_4$/Pt heterostructure

Haomang He(何浩茫), Ruijie Xu(徐睿劼), Anke Song(宋安柯), Zhongqiang Chen(陈中强), and Xuefeng Wang(王学锋)

Chin. Phys. B, 2026, 35 (**1**): 017502. DOI: 10.1088/1674-1056/ae181c

Chemical pressure manipulation of ferromagnetism in magnetic semiconductor $Ba(Zn,Mn,Cu)_2As_2$

Xueqin Zhao(赵雪芹), Jinou Dong(董金瓯), Lingfeng Xie(谢玲凤), Xun Pan(潘洵), Haoyuan Tang(唐浩原), Zhicheng Xu(徐之程), and Fanlong Ning(宁凡龙)

Chin. Phys. B, 2025, 34 (**10**): 107510. DOI: 10.1088/1674-1056/addbce

Complex magnetic and transport properties of $EuBi_2$ single crystal

Ping Su(苏平), Hui Liang(梁慧), Yi-Ran Li(李祎冉), Huan Wang(王欢), Na Li(李娜), Kai-Yuan Hu(胡开源), Ying Zhou(周颖), Dan-Dan Wu(吴丹丹), Yan Sun(孙燕), Qiu-Ju Li(李秋菊), Jin-Jin Hong(洪锦锦), Xia Zhao(赵霞), Xue-Feng Sun(孙学峰), and Yi-Yan Wang(王义炎)

Chin. Phys. B, 2025, 34 (**6**): 067503. DOI: 10.1088/1674-1056/adca17

Unconventional room-temperature negative magnetoresistance effect in Au/n-Ge:Sb/Au devices

Xiong He(何雄), Fan-Li Yang(杨凡黎), Hao-Yu Niu(牛浩峪), Li-Feng Wang(王立峰), Li-Zhi Yi(易立志),Yun-Li Xu(许云丽), Min Liu(刘敏), Li-Qing Pan(潘礼庆), and Zheng-Cai Xia(夏正才)

Chin. Phys. B, 2024, 33 (**3**): 037504. DOI: 10.1088/1674-1056/ad15f8

Coexistence of room-temperature negative differential resistance and unsaturated magnetoresistance effects in germanium-based devices

Xiong He(何雄)[1,†], Ling Cai(蔡玲)[1], Li-Zhi Yi(易立志)[1],
Guang-Duo Lu(鲁广铎)[1], Li-Qing Pan(潘礼庆)[1,‡], and Zhi-Gang Sun(孙志刚)[2]

[1] *Hubei Engineering Research Center of Weak Magnetic-field Detection, College of Science, China Three Gorges University, Yichang* 443002, *China*
[2] *Material Science and Engineering School, Taiyuan University of Science and Technology, Taiyuan* 030024, *China*

(Received 14 March 2025; revised manuscript received 20 August 2025; accepted manuscript online 21 August 2025)

We demonstrate room-temperature negative differential resistance (NDR) and unsaturated magnetoresistance (MR) effects in germanium-based devices. Our findings indicate that the observed NDR primarily originates from the carrier injection effect induced by local impact ionization in germanium. As the magnetic field increases, the MR values exhibit an unsaturated behavior, increasing quadratically at low fields and transitioning to a linear increase at higher fields, reaching approximately 91% at 1 T. We attribute this large unsaturated MR to carrier inhomogeneity. The equivalent Hall electric field strength was used to characterize the degree of carrier inhomogeneity under magnetic fields: a larger equivalent Hall electric field strength indicates stronger carrier inhomogeneity and consequently a larger corresponding MR. The coexistence of excellent room-temperature NDR and large unsaturated MR in germanium-based devices (achieved by constructing electrodes at two edge positions on the semiconductor surface) enables the development of multifunctional devices.

Keywords: germanium-based devices, magnetoresistance, negative differential resistance, electrical transport

PACS: 75.47.–m, 85.30.–z, 83.60.Np

DOI: 10.1088/1674-1056/adfdc3 **CSTR:** 32038.14.CPB.adfdc3

1. Introduction

The negative differential resistance (NDR) effect has significant applications in electronic amplifiers, oscillators, memories and logic functions, among others. Currently, NDR has been observed in a large number of materials and their corresponding devices, such as Ge,[1–11] Si[12–15] and NbO_x.[16,17] Among these, NDR in Ge-based devices arises from either the effect of the heterojunction interface or from the intrinsic bulk material properties. Apart from research on amorphous Ge at room temperature,[5] observations of bulk NDR in Ge-based devices have primarily been reported in low-temperature environments. Indeed, investigations into its regulation have shown that an enhancement of the NDR effect is observed under external magnetic fields.[10–13]

Magnetoresistance (MR) devices have been widely applied in information storage, magnetic sensing and other fields. In addition to giant MR, tunnel MR and colossal MR based on magnetic materials, researchers have also focused considerable attention on the MR effect in devices based on non-magnetic materials, such as Ge,[10,11,18–28] Si,[29–36] GaAs,[37,38] WTe_2,[39] silver chalcogenides,[40] and so on. Among these, the MR research on Ge-based devices at room temperature has theoretical and applied significance. However, the physical mechanisms underlying MR effects are diverse, including the carrier inhomogeneity model caused by space charge effects,[26] the diode-assisted geometric enhancement model,[20] the carrier recombination model based on local impact ionization in the space-charge region,[18] the dependence of measured positive and negative MR values on the distance of the voltage probe arising from the trapezoidal distribution of space-charge regions,[24] the rectification MR[21–23] and so forth. Further research on the intrinsic physical mechanism governing the MR effect in Ge-based devices at room temperature may be beneficial for advancing its practical application.

Recently, He *et al.*[12] reported the simultaneous observation of NDR and unsaturated MR effects in an In/SiO_2/p-Si/SiO_2/In heterojunction device below 25 K. Nevertheless, within the NDR conductive region, the MR values tended to saturate. In addition, in an Ag/p-Ge:Ga/Ag device, the coexistence of NDR and unsaturated MR was observed, and the evolution of NDR with different magnetic field strengths was systematically studied.[10] However, the internal mechanism and co-regulation method of the coexistence of NDR and unsaturated MR in Ge-based devices still need to be further explored.

In this paper, In/p-Ge:Ga/In devices are fabricated and the coexistence of room-temperature NDR and unsaturated MR in the devices is discovered. Through a systematic comparative analysis of the equivalent Hall effect corresponding to different measurement methods and different devices, this work reveals the formation mechanism of the NDR effect and the

†Corresponding author. E-mail: hexiong@ctgu.edu.cn
‡Corresponding author. E-mail: lpan@ctgu.edu.cn

© 2026 Chinese Physical Society and IOP Publishing Ltd. All rights, including for text and data mining, AI training, and similar technologies, are reserved.

methods regulating its coexistence with large unsaturated MR, establishing an approach to achieve superior NDR and MR performance in Ge-based devices.

2. Experimental details

A single polished p-Ge:Ga crystal wafer (with room-temperature resistivity ρ of 10–30 Ω·cm and a thickness of 500 μm) was used. The wafer was cut into rectangular shapes of about 11.9 mm×4.0 mm (called a longer sample) and 3.4 mm×3.0 mm (called a shorter sample) for electric transport measurements, and 8 mm×8 mm for van der Pauw measurements. To investigate the influence of electrode distance on the electrical transport properties, we selected the longer sample and soldered four In electrodes (labeled 1–4) on the polished surface; thus a longer In/p-Ge:Ga/In device was obtained. The schematic diagram of the longer device is shown in Fig. 1(a). The average spacing between electrodes is L_{ij} (i, j = 1–4), where $L_{43} \approx 8.88$ mm, $L_{42} \approx 5.18$ mm, $L_{41} \approx 2.15$ mm and $L_{12} \approx 1.85$ mm. For the shorter samples, one was applied to fabricate a shorter In/p-Ge:Ga/In device with In electrodes on the edge of the polished surface (see Fig. 1(b)). The other was used to apply In electrodes on both sides of the sample (see Fig. 1(c)). We labeled these as devices NU0# and U0#, respectively. The electrical transport characteristics, namely the V–I and R–B characteristics, were obtained using the two-probe method with a current source (Keithley 622X) and a voltmeter (Keithley 2182A). After completing measurement of the V–I characteristic curve under each constant magnetic field, a brief waiting period to mitigate possible thermal effects was allowed. The variable temperature measurement was completed in a commercial low-temperature and low-magnetic-field electrical transport measurement (LTLM) system, which can control the device at a constant temperature so we can ignore the temperature changes that may occur during the measurement. The measured voltages between electrodes of the longer device are denoted as V_{ij}. The carrier density (p) and mobility (μ_p) of the p-Ge:Ga were approximately 2.6×10^{14} cm^{-3} and 2×10^3 cm^2·V^{-1}·s^{-1}, respectively, as measured by the van der Pauw method. Opposite magnetic fields (labeled as B_+ and B_-) were parallel to the sample surface and perpendicular to the direction toward the two electrodes (see Figs. 1(a)–1(c)).

3. Results and discussion

As shown in Fig. 1(d), we find that the V–I characteristics are straight lines passing through the origin, suggesting that the contact between In and p-Ge:Ga is ohmic. Figure 1(e) and 1(f) present the V_{43}–I characteristics under different magnetic fields. The details of the V_{43}–I characteristics are presented in the supplementary material (Figs. S1(a1)–S1(a4)). At small applied currents, the V_{43}–I characteristics for both magnetic field directions exhibit the expected symmetry relative to the V_{43}–I characteristics at zero magnetic field (see Figs. 1(e), S1(a1) and S1(a2)). However, as shown in Figs. 1(f), S1(a3) and S1(a4), at large applied current this symmetry disappears. Meanwhile, the measured voltage increases with increasing magnetic field in the direction of B_+, while it decreases with increasing magnetic field in the direction of B_-. This indicates that positive and negative MR are observed in the B_+ and B_- directions, respectively. The MR is defined as MR $= [R(B) - R(0)] \times 100\%/R(0) = [V(B) - V(0)] \times 100\%/V(0)$, where $R(B)$ and $R(0)$ are the resistances of the device under an applied magnetic field and zero magnetic field, respectively. $V(B)$ and $V(0)$ are the measured voltages with and without an applied magnetic field, respectively. Similarly, these kinds of symmetry, asymmetry and negative MR are also observed in the V_{41}–I characteristics in the direction of B_+ and B_- (see Figs. S1(b1)–S1(b4) in the supplementary material).

According to previous work,[18] the asymmetry may be related to surface imperfections on the sample, but the measurement of negative MR was not observed. Furthermore, although distinct defects on the upper and lower surfaces of the device modify the carrier recombination rate[18] they are unlikely to induce equivalent charge accumulation analogous to that suppressed under pulsed high magnetic fields.[28] As a result, the negative MR effect is significantly alleviated. Thus, this surface imperfection is not the main reason for the negative MR observed in our work, even though we use a similar single polished device. Compared with previously reported similar device structures,[18] we employ a relatively lower magnetic field range and utilize a current source instead of a voltage source. The choice of power source significantly affects transport properties, particularly the formation of NDR effects.[10,41] The measured negative MR reported by Cheng *et al.*[24] was regulated by the distance of the voltmeter probe due to the trapezoidal distribution of the space-charge region. However, since we employed the two-probe method to measure the MR properties, this voltmeter probe distance-dependent effect reported by Cheng *et al.*[24] is not present in our work. Considering the raw MR data, which might be mixed with the Hall effect and lead to the asymmetry of MR, the asymmetry and measured negative MR in our work might be also related to Hall effect. In order to analyze the influence of the Hall effect on the electrical transport properties of the device, we selected positions M and N for schematic illustration of the current direction (see Figs. 1(g)–1(i)). Here, the In electrodes were positioned on the polished surface. A significant accumulation of holes and electrons was observed at points M and N. The current in the y direction is not considered since it is parallel to the magnetic field. When $B = 0$ T, if the angle between the current I and the z direc-

tion is θ, then $I_z = I \cdot \cos\theta$. After applying a positive magnetic field B_+, the electrons or holes will be deflected by an angle γ (i.e., the Hall angle), and then $\alpha = \theta - \gamma$. The directions of Hall voltage corresponding to positions M and N are the same, so the Hall voltage corresponding to I_z under magnetic field B_+ is $V_H = (R_H B/d) \cdot I_z = 2(R_H B/d) \cdot I \cdot \cos\alpha$, where R_H is the Hall coefficient of Ge and d is the length of the sample along the direction of the magnetic field. Then, the direction of the voltage corresponding to MR (labeled as V_R) is the same as that of V_H, so the measured voltage $V(B_+)$ can be expressed as $V(B_+) = V_R + V_H = V_R + 2(R_H B/d)I \cdot \cos\alpha$. Similarly, under the condition of B_-, $\beta = \theta + \gamma$ and $V(B_-) = V_R - 2(R_H B/d) \cdot I \cdot \cos\beta$. Obviously, the values of $V(B_+)$ and $V(B_-)$ are different when $B \neq 0$ T, resulting in asymmetry of the V–I characteristics with respect to zero magnetic field, especially in the large current range. Meanwhile, under the B_- magnetic field condition, the value of $V(B_-)$ may be smaller than $V(0)$. Thus, measured negative MR can be observed. In device U0#, part of the In electrode remains on the surface of the device during the soldering process. This creates an additional current component I_z, producing a similar influence of the Hall effect. Therefore, in the following research in this work we applied the formula $V_{even} = (V(B_+) + V(B_-))/2$ to eliminate the influence of the Hall effect. Meanwhile, the formula $V_H(B) = (V(B_+) - V(B_-))/2$ was used to obtain the Hall voltage $V_H(B)$ under magnetic field B. Considering that this method is not a conventional method for obtaining the Hall effect, we label the Hall effect obtained by this method as the 'equivalent Hall effect'.

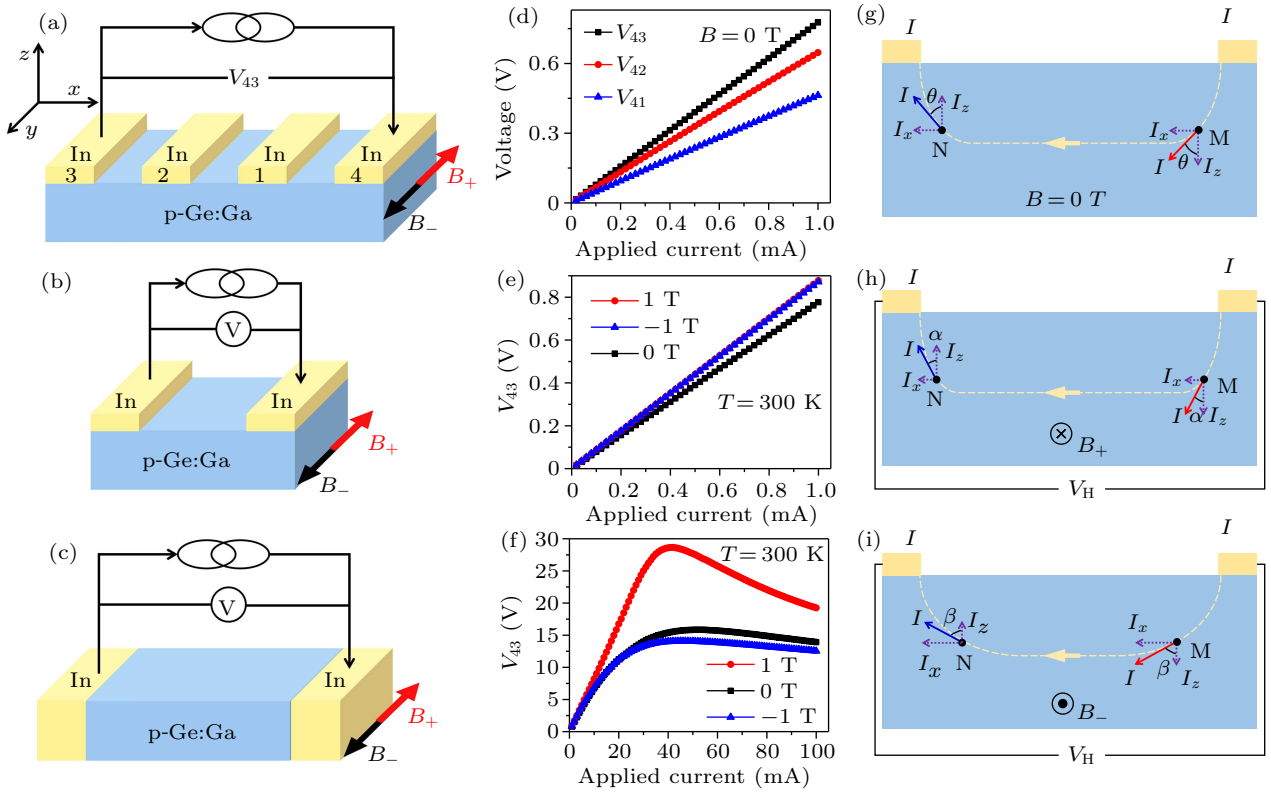


Fig. 1. Schematic measurement diagrams, measurement results of electrical transport properties before eliminating the Hall effect and schematic diagrams of the current direction in the device. (a) Schematic measurement diagram between the fourth and third electrodes of the longer In/p-Ge:Ga/In device. (b), (c) Schematic measurement diagrams of the two shorter (NU0# and U0#) In/p-Ge:Ga/In devices, respectively. (d) The V–I characteristics of the longer device measured between electrodes i and j at zero field. (e), (f) The V–I characteristics of the longer device measured between the fourth and third electrodes in different current ranges under different magnetic fields at B_+ and B_- directions, respectively. (g)–(i) Schematic diagrams of the current directions at zero field, B_+ and B_- magnetic fields at positions M near the anode and N near the cathode, respectively.

Figures 2(a1) and 2(b1) show the V–I characteristics of the longer device measured between electrodes i and j at zero field. When the currents are in the ranges of about 0–10 mA and 0–5 mA, respectively, the measured voltage increases linearly with increase in the applied current, presenting ohmic characteristics. We define these current ranges as ohmic regions. As the current increases further, the measured voltage exhibits a non-linear behavior. Before the voltage reaches the peak value (denoted as V_{peak}), the relationship between I and V is not an ideal quadratic relationship, indicating that the electrical transport characteristics may not be simply controlled by the space-charge effect. Even though the breakdown field in bulk Ge is as high as about 10^5 V·cm^{-1},[42] the non-uniform distribution of electric field lines means that the electric field strength near the electrodes is sufficient to trigger local impact ionization.[10] Therefore, this non-linear region corresponds to the coexistence of the space-charge effect and local impact ionization. We define this current region as the space-charge effect and local impact ionization coexistence region. As shown in Fig. 2(a1), as the current continues to increase,

the measured voltage gradually decreases, showing a NDR effect. The value of $V_{\rm peak}/V_{100\ \rm mA}$ is about 1.14. Compared with the V_{43}–I characteristics obtained at a larger electrode distance, the $V_{\rm peak}/V_{100\ \rm mA}$ value (only about 1.003) is significantly smaller at smaller electrode distances (see Figs. 2(a1) and 2(b1)), indicating that by adjusting the electrode distance on the same surface, the room-temperature NDR effect of Ge-based devices can be regulated. Figures 2(c1) and 2(d1) show the V–I characteristics of devices NU0# and U0#, respectively, at zero field. The NDR effect can be found in device NU0# ($V_{\rm peak}/V_{100\ \rm mA} = 1.08$) but it cannot be observed in device U0# ($V_{\rm peak}/V_{100\ \rm mA} = 1$). This indicates that Joule heating may be not the main physical mechanism for NDR since the geometric size of the two shorter devices is about the same. In addition, the temperature dependence of NDR obtained in the LTLM system (see Fig. S2 in the supplementary material) is similar to that reported in the literature,[10] i.e., $V_{\rm peak}$, and its corresponding threshold current increases with decrease in temperature, demonstrating that Joule heating is indeed not the primary cause of NDR formation. Since the measurement is completed in a vacuum environment, the effect of humidity on the formation of NDR can also be ignored.[10,43]

The V–I characteristics under different magnetic fields are shown in Figs. 2(a2), 2(b2), 2(c2) and 2(d2). More details on the V–I characteristics are presented in the supplementary material (Figs. S3(a1), S3(b1), S3(c1) and S3(d1)). The values of $V_{\rm peak}$ increase with increasing applied magnetic field (see Figs. 2(a2), 2(b2) and 2(c2)). Meanwhile, the values of $V_{\rm peak}/V_{100\ \rm mA}$ also increase with increasing magnetic field. In addition, in device U0#, NDR only occurs when $B \geq 0.5$ T, and the ratio $V_{\rm peak}/V_{100\ \rm mA}$ increases with magnetic field strength (see Fig. 2(d2)). These results suggest that the NDR effect is significantly enhanced by an applied magnetic field.

Figures 2(a3), 2(b3), 2(c3) and 2(d3) illustrate the different distribution characteristics of electric field lines. Firstly, when the In electrodes are on the edge of the sample surface, the electric field lines are distributed non-uniformly and restricted by the edge of the device. Furthermore, for the fourth and first electrodes, the electric field lines remain non-uniform, but their confinement by the edges of the device is relatively weaker. Finally, in device U0# the electric field lines are almost uniformly distributed. Non-uniform distribution of electric field lines in the devices is conducive to the formation of a large local electric field strength, resulting in the occurrence of local impact ionization in Ge. Therefore the NDR effect occurs easily when the electrodes are distributed on the edge of the sample surface.

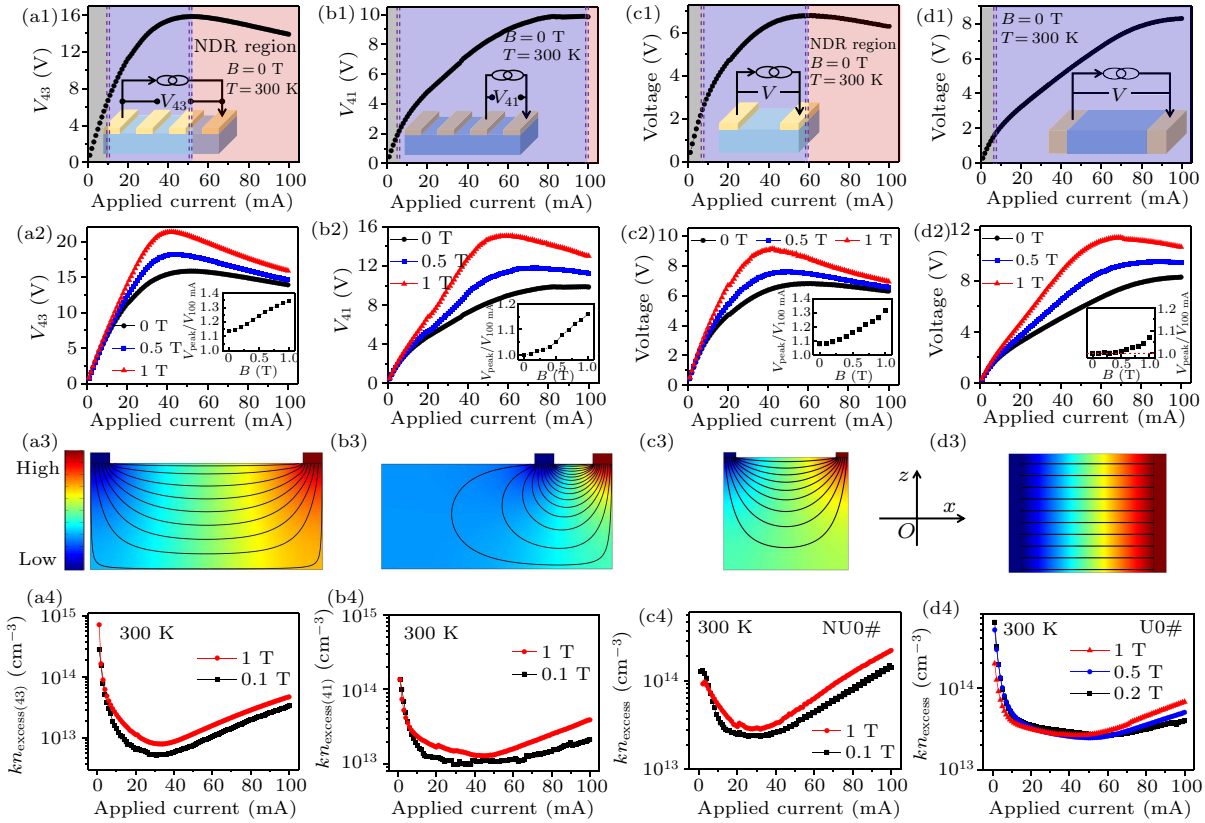


Fig. 2. (a1)–(a4), (b1)–(b4) The properties measured between fourth and third, and fourth and first electrodes of the longer device, respectively. (c1)–(c4), (d1)–(d4) The properties of the shorter devices NU0# and U0#, respectively. (a1), (b1), (c1), (d1) The V_{41}–I characteristics at 0 T. (a2), (b2), (c2), (d2) The V–I characteristics after eliminating the Hall effect under different magnetic fields, with insets showing the corresponding $V_{\rm peak}/V_{100\ \rm mA}$–$B$ characteristics. The V–I characteristics measured under 0.2–0.4 T and 0.6–0.9 T are shown in Figs. S3(a1), S3(b1), S3(c1) and S3(d1) in the supplementary material. (a3), (b3), (c3), (d3) Schematic diagrams of the distributions of electric field lines. (a4), (b4), (c4), (d4) The $kn_{\rm excess}$–I characteristics under different magnetic fields.

To further analyze the possible intrinsic physical mechanism of NDR, we estimated the excess carrier density (n_{excess}). n_{excess} can be expressed as $n_{\text{excess}} = n_{\text{p}} - n_{\text{e}} = 1/qR_{\text{H}}$.[44] q, n_{p} and n_{e} are the amount of charge, the hole density and the electron density, respectively. We still apply the position points M and N as examples. According to the above analysis, the equivalent $V_{\text{H}}(B)$ is expressed as

$$V_{\text{H}}(B) = \frac{V(B_+) - V(B_-)}{2} = 4(R_{\text{H}}B/d)I\cos\theta\cos\gamma. \quad (1)$$

The values of equivalent V_{H} are positive at B_+ (see Figs. S3(a2), S3(b2), S3(c2) and S3(d2) in the supplementary material), indicating that the dominant charge carriers are holes, which is consistent with the p-type Ge semiconductor used. We can use Eq. (1) to substitute R_{H} into the equation $n_{\text{excess}} = 1/qR_{\text{H}}$ to obtain

$$n_{\text{excess}} = 4\cos\theta\cos\gamma\frac{BI}{qV_{\text{H}}(B)d}. \quad (2)$$

If k is defined as $k = \frac{1}{4\cos\theta\cdot\cos\gamma}$, then

$$kn_{\text{excess}} = \frac{BI}{qV_{\text{H}}(B)d}. \quad (3)$$

k is related to the Hall angle γ, and $\tan\gamma = \mu_{\text{p}}B$, where $\mu_{\text{p}} = 2\times10^3$ cm$^2\cdot$V$^{-1}\cdot$s^{-1}, indicating that k is independent of the applied current I. The kn_{excess}–I characteristics are shown in Figs. 2(a4), 2(b4), 2(c4) and 2(d4). We analyze NDR formation under a low magnetic field (similar to the zero-field case), since the Lorentz force induces only weak carrier deflection at such low fields. The value of kn_{excess} initially decreases with increasing current due to minority electron injection from the electrodes.[10,34,35,44] With further increase in the applied current, kn_{excess} begins to rise. This indicates that local impact ionization occurs and generates plenty of effective carriers. This effective carrier injection effect is similar to that in previous works.[10,15,45] Considering constant carrier mobility at room temperature, the device resistance is inversely proportional to kn_{excess}. When the electrodes are distributed on the edge of the sample, the increased amplitude of kn_{excess} is larger (see Figs. 2(a4) and 2(c4)). kn_{excess} increases slowly with increasing the applied current of the longer device in the fourth and first electrodes case and in device U0# (see Figs. 2(b4) and 2(d4)). Since the increment of kn_{excess} corresponds exactly to the formation of NDR in the different devices, the NDR effect in this work is mainly derived from the carrier injection effect caused by local impact ionization in Ge. The consistency between our conclusion and previous Hall measurements results[10] confirms the validity of the 'equivalent Hall effect' extraction approach proposed here. Based on the above discussion, replacing the substrate with highly doped p-Ge:Ga impedes the formation of a similar inhomogeneous electric field distribution within the device. Consequently, this prevents the triggering of localized impact ionization in Ge, ultimately hindering formation of the NDR effect. Indeed, the V–I characteristics of the highly doped samples (see Fig. S4) exhibit no observable nonlinearity.

When $B = 1$ T, the value of kn_{excess} increases more obviously after reaching the minimum value, indicating that the carrier injection effect is stronger. Thus, the NDR effect is enhanced after applying a high enough magnetic field. Analysis indicates that under an applied magnetic field, Lorentz deflection of carriers increases the probability of carrier–carrier impact ionization, thereby enhancing carrier injection. Therefore, the NDR effect can be enhanced by an applied magnetic field.

Under constant-current conditions, with increasing magnetic field strength, the measured voltage gradually increases, illustrating a positive MR. From the MR–I characteristics (see Fig. 3), we observe that MR increases first with increasing I. When I increases to the current corresponding to V_{peak}, MR reaches a maximum. As the current continues to increase, MR decreases. Through comparison of the MR_{max} values we mainly find the following three phenomena. Firstly, MR_{max} increases with decreasing electrode distance in the longer device. This indicates that when electrodes are on the same surface of the sample, a relatively larger MR can be obtained with a smaller electrode distance, which is similar to the results reported previously.[30] Secondly, under the same geometric size conditions, the difference in the electric field distribution at zero field formed by different electrode distributions can induce a difference in MR. Finally, when the electrodes are distributed on the edge of the sample surface, the geometric size of the samples has an influence on the MR. This is similar to the MR properties of geometrically controlled nonmagnetic semiconductor-based devices reported in the previous literature.[20,34,46] Considering that there are differences in the range of the conduction regions under different magnetic fields, we divide the three conductive regions, i.e., ohmic, space-charge effect and coexistence of local impact ionization, and NDR regions by the characteristics of the V–I characteristics at 1 T. In the region of coexistence of space-charge and local impact ionization, the values of MR are also significantly larger. So, our results provide further evidence for the point that MR effects based on the space-charge effect[35] or impact ionization effect[47,48] can be significantly enhanced. Furthermore, the trends of the equivalent Hall electric field strength E_{H} ($E_{\text{H}} = V_{\text{H}}(B)/L_{ij}$) values with I are similar to those of MR values with I (see Fig. 3).

As shown in Fig. 4, $E_{\text{H(max)}}$ is positively related to MR_{max}. According to Eq. (3), we can obtain

$$E_{\text{H}} = \frac{BI}{qdL_{ij}}\frac{1}{kn_{\text{excess}}}, \quad (4)$$

indicating that the equivalent value of E_{H} is inversely pro-

portional to that of kn_{excess} under the same current conditions. According to previous results,[37,49] in non-magnetic semiconductor-based devices with a lower intrinsic carrier concentration, a larger MR can easily be obtained. Consistent with expectations, we observe that in a certain measurement case the trend of kn_{excess} changing with I is opposite to that of MR varying with I (see Figs. 2(a4), 2(b4), 2(c4), 2(d4) and 3). In different measurement cases, it is difficult for us to find the correlation between kn_{excess} and MR since the values of k are different from each other. For the longer device, where the electrodes are on the same surface of the sample and the electric field lines are restricted relatively weakly by the edge of the device, it is easier to induce deflection of the electrons and holes after applying the magnetic field. This indicates that the change in carrier inhomogeneity distribution is stronger, resulting in a larger MR. Therefore, $\text{MR}_{(12)\,\text{max}} > \text{MR}_{(41)\,\text{max}} > \text{MR}_{(42)\,\text{max}} > \text{MR}_{(43)\,\text{max}}$. Among these, the largest MR_{max} value is about 91% at 1 T, corresponding to the measurement results between the first and second electrodes of the longer device. The highest MR_{max} value is comparable to that of MR in the In/Ge/In structured device,[26] and larger than the rectification MR in the Al/Ge Schottky heterojunction device[23] at 1 T. For the shorter NU0# and U0# devices there is a significant difference in the distribution of electric field lines under zero magnetic field. When a magnetic field is applied, the degree of change in carrier inhomogeneity in device U0# is larger than that of NU0#, resulting in $\text{MR}_{(\text{U0\#})\,\text{max}} > \text{MR}_{(\text{NU0\#})\,\text{max}}$. Based on the above analyses, the value of the equivalent E_{H} may be applied to characterize the degree of carrier inhomogeneity. Critically, as devices scale to micro/nano dimensions, the correlation between MR_{max} and $E_{\text{H(max)}}$ requires further investigation.

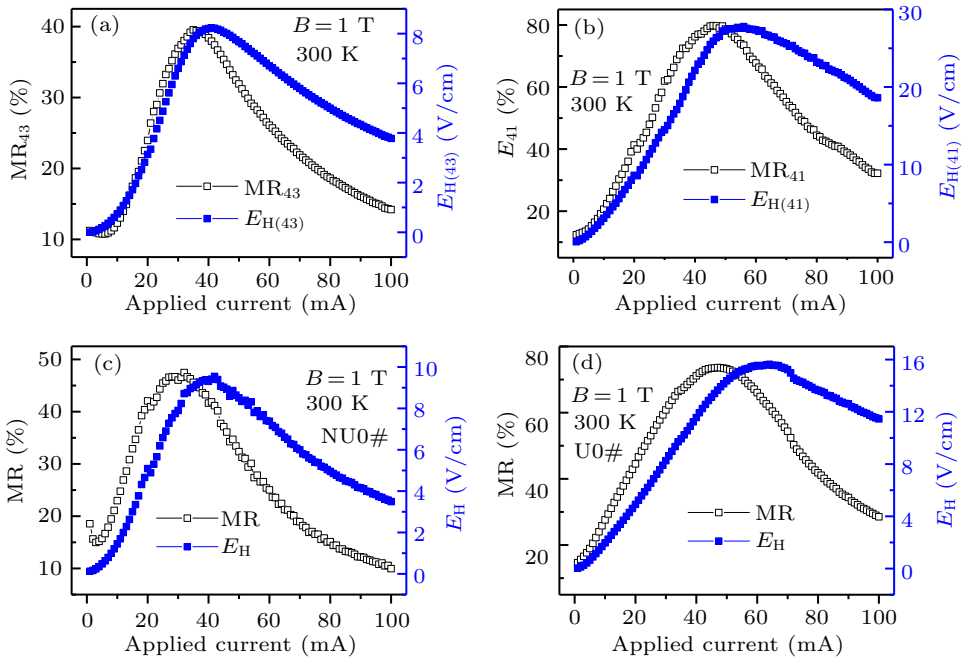


Fig. 3. Evolution of calculated MR and E_{H} of different devices with current. (a), (b) The calculated MR–I and E_{H}–I characteristics obtained in fourth and third, and fourth and first electrodes cases of the longer device, respectively. (c), (d) The calculated MR–I and E_{H}–I characteristics of the shorter devices NU0# and U0#, respectively.

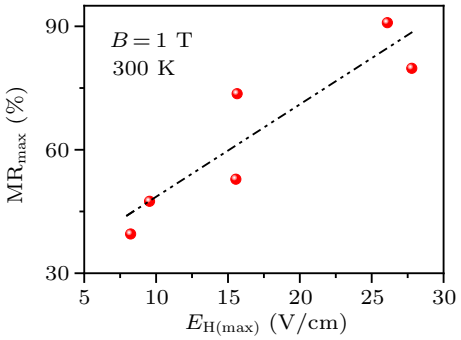


Fig. 4. MR_{max} versus $E_{\text{H(max)}}$ corresponding to different measurement cases and devices under 1 T at room temperature.

To analyze the behavior of MR, we present the calculated MR–B characteristics in Figs. 5(a)–5(d). All the MR–B characteristics are well fitted by the formula $\text{MR} = (\mu_{\text{MR}}B)^2$ below 0.3 T, where μ_{MR} relates to MR mobility. The value of μ_{MR} is close to that of the carrier mobility measured by the van der Pauw method. This normal quadratic dependence originates from the deflection of the carrier trajectory under a magnetic field.[44,50,51] When $B > 0.3$ T, the MR increases linearly with increasing magnetic field. This quadratic and then linear relationship has also been reported in other non-magnetic semiconductor material devices.[52] It is noteworthy that even in the NDR conductive region ($I = 80$ mA and 100 mA as examples), the MR is also unsaturated, indicating that coexistence of NDR and unsaturated MR is realized.

To further study the influence of electrode position on the

NDR and MR properties of the obtained device, we studied the electrical transport properties of the longer device in the case of electrode pairs 4–1 and 1–2. As expected, we can easily observe NDR in the V_{42}–I characteristics, and NDR can only be found in the V_{12}–I curve under a higher magnetic field (see Figs. S5(a) and S5(b)). Moreover, the NDR phenomenon can also be enhanced with increase in the magnetic field. Not only that, the trend of E_H with I is also consistent with that of MR with I (see Figs. S5(c) and S5(d)). MR_{42} and MR_{12} also increase quadratically and then linearly with increasing magnetic field (see Figs. S5(e) and S5(f)). Considering the relatively large MR observed for electrode pairs 1–2 of the longer device, we measured the R–B characteristics in different conductive regions at room temperature to study the MR properties (see Fig. 5(e)). Similarly, the R–B characteristics are symmetric by reversing the direction of the magnetic field in the ohmic region, but become asymmetric characteristics when induced by the Hall effect. After eliminating the influence of the Hall effect on resistance, we obtain the corresponding calculated MR–B characteristics (see Fig. 5(f)). The smaller values of MR in Fig. 5(f) compared with Fig. S5(f) originate from differences in Joule heating. This occurs because a constant current is applied throughout the R–B measurement process while the current values for the V–I measurement are obtained from the V–I characteristics under each magnetic field.[12] The former more easily accumulates Joule heating. It can be seen from Fig. 5(f) that, in the NDR region, the MR values increase quadratically at first and then linearly with increasing magnetic field.

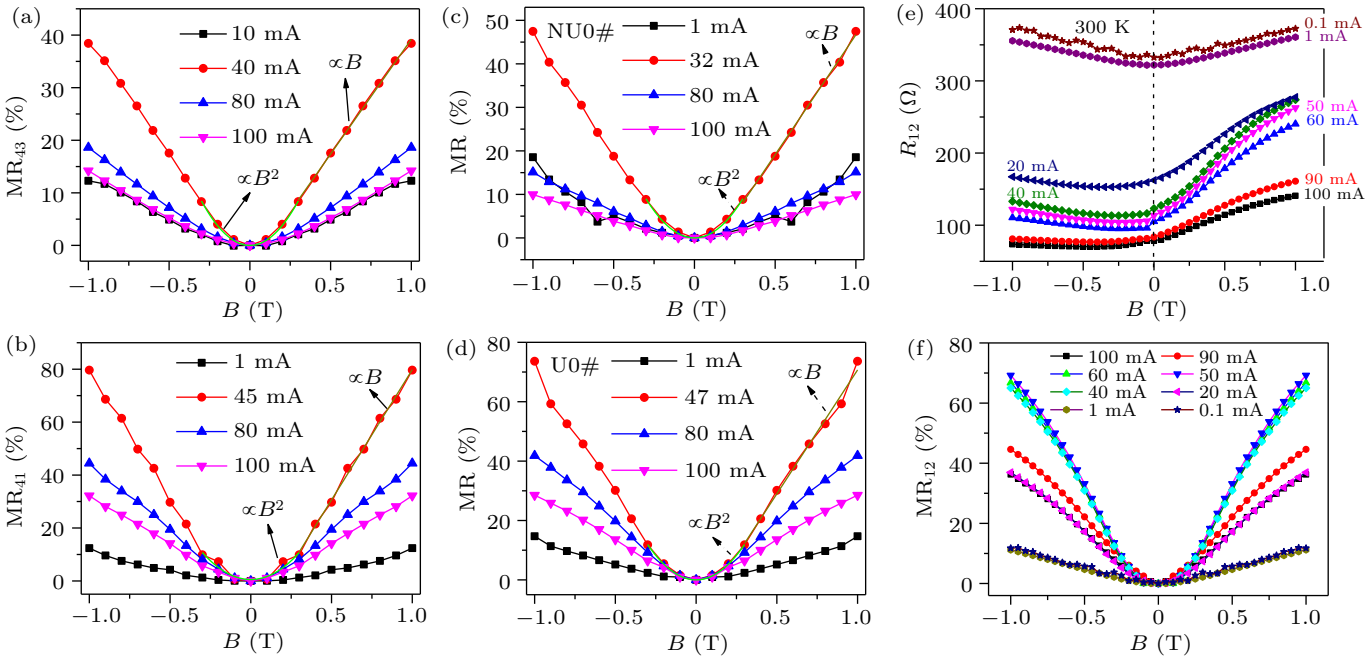


Fig. 5. The calculated MR properties of different devices at room temperature. (a), (b) The calculated MR–B characteristics obtained in fourth and third, and fourth and first electrode cases for the longer devices, respectively. (c), (d) The calculated MR–B characteristics of the shorter NU0# and U0# devices, respectively.

Table 1. MR and NDR properties of the longer devices with different electrode connection modes and the shorter devices (NU0# and U0#).

Device		MR properties		NDR properties	
		MR_{max}	MR values in NDR region at 80 mA and 1 T	$V_{peak}/V_{100\ mA}$ at 0 T	$V_{peak}/V_{100\ mA}$ at 1 T
Longer devices	Electrode pair 4–3	40%	18%	1.1384	1.3438
	Electrode pair 4–2	53%	28%	1.0527	1.2433
	Electrode pair 4–1	80%	45%	1.0030	1.1583
	Electrode pair 1–2	91%	35%	1.0000	1.0749
Shorter devices	NU0#	47%	15%	1.0793	1.3156
	U0#	74%	42%	1.0000	1.0688

From Table 1, it is evident that it is difficult to obtain excellent NDR properties for electrode pairs 4–1 and 1–2 in the longer device, as well as for device U0#. In these electrode structures, the electric field distribution at at least one electrode position does not experience significant edge restriction, or the field mainly has a uniform electric field distribution. Consequently, with devices based on these electrode structures it will be relatively difficult to achieve simultane-

ous coexistence of excellent NDR and unsaturated MR. Fortunately, when the electrodes are positioned at both edges of the sample surface (corresponding to electrode pair 4–3 in the longer device and device NU0#), it is relatively easy to achieve coexistence of excellent NDR and unsaturated MR. Furthermore, the MR properties within the NDR conduction region do not vary significantly with device size, although the corresponding value of MR_{max} is not the highest. Meanwhile, the NDR properties remain stable. Therefore, based on the above discussions, for batch engineering applications we recommend fabricating metal electrodes on two edge positions on the semiconductor surface to facilitate simultaneous achievement of excellent NDR properties and a large unsaturated MR.

4. Conclusion

In conclusion, we investigated room-temperature NDR and MR effects in In/p-Ge:Ga/In devices. Our analysis indicates that the observed NDR primarily originates from the carrier injection effect induced by local impact ionization within Ge. The MR exhibits an unsaturated behavior, increasing quadratically with magnetic field at lower fields before transitioning to a linear increase at higher fields, reaching a significant value of approximately 91% at 1 T. This large unsaturated MR is probably associated with carrier inhomogeneity. Furthermore, the equivalent Hall electric field strength is positively correlated with the MR properties, suggesting its potential utility in characterizing the degree of carrier inhomogeneity. Notably, unsaturated MR persists even within the NDR region, highlighting the potential for developing multifunctional devices that leverage the coexistence of both NDR and unsaturated MR effects. Finally, we demonstrate that fabricating metal electrodes at two edge positions on the semiconductor surface is beneficial for the simultaneous achievement of excellent NDR properties and large unsaturated MR.

Acknowledgements

This work was supported in part by the Youth Program of Natural Science Foundation of Hubei Province (Grant No. 2024AFB333), Natural Science Foundation of Yichang (Grant No. A24-3-021), the Special Funding for Talents of China Three Gorges University (Grant No. 8230202), and the National Natural Science Foundation of China (Grant No. 12274258).

References

[1] Park Y D, Wilson A, Hanbicki A T, Mattson J E, Ambrose T, Spanos G and Jonker B T 2001 *Appl. Phys. Lett.* **78** 2739
[2] Brunbauer F M, Bertagnolli E and Lugstein A 2015 *Nano Lett.* **15** 7514
[3] Kagan M S, Kalashnikov S G and Zhdanova N G 1967 *Physica Status Solidi (b)* **24** 551
[4] Kroemer H 1964 *Proc. IEEE* **52** 1736
[5] Okunev V D 1980 *Soviet Physics Journal* **23** 265
[6] McGroddy J C 1970 *IEEE Transactions on Electron Devices* **17** 207
[7] DeBiasi R S and Yee S S 1970 *Proc. IEEE* **58** 256
[8] Paige E G S 1969 *IBM Journal of Research and Development* **13** 562
[9] Fawcett W 1967 *Electronics Letters* **3** 505
[10] He X, Xia Z C, Niu H Y, Song Y J, Zeng Z, Jiang D Q, Liang Y Y and Huang H 2022 *physica status solidi (RRL) - Rapid Research Letters* **16** 2200165
[11] He X, Xia Z C, Niu H Y and Zeng Z 2022 *Journal of Materials Science & Technology* **114** 1
[12] He X, Yang Z, Zhu C, He B, Luo F, Wei P, Zhao W Y, Wang J F and Sun Z G 2020 *J. Phys.: Condens. Matter* **32** 305701
[13] Danilyuk A L, Trafimenko A G, Fedotov A K, Svito I A and Prischepa S L 2016 *Appl. Phys. Lett.* **109** 222104
[14] Liu X, Mi W, Zhang Q and Zhang X 2019 *Appl. Phys. Lett.* **114** 242402
[15] Liu W, Guo H, Li W, Wan X, Bodepudi S C, Shehzad K and Xu Y 2018 *Appl. Phys. Lett.* **112** 201109
[16] Nath S K, Nandi S K, El-Helou A, Liu X, Li S, Ratcliff T, Raad P E and Elliman R G 2020 *Phys. Rev. Appl.* **13** 064024
[17] Nandi S K, Nath S K, El-Helou A E, Li S, Liu X, Raad P E and Elliman R G 2019 *Advanced Functional Materials* **29** 1906731
[18] Chen J J, Piao H G, Luo Z C and Zhang X Z 2015 *Appl. Phys. Lett.* **106** 173503
[19] Lidsky D, Hutchins-Delgado T, Sharma P, Dobrosavljevic V and Lu T M 2025 *Appl. Phys. Lett.* **126** 092104
[20] Chen J J, Zhang X Z, Piao H G, Wang J M and Luo Z C 2014 *Appl. Phys. Lett.* **105** 193508
[21] Huang Q K, Wang J, Lu S Y, Chen Y X, Bai L H, Dai Y Y, Tian Y F and Yan S S 2018 *ACS Applied Materials & Interfaces* **10** 24905
[22] Huang Q K, Yan Y, Zhang K, Li H H, Kang S and Tian Y F 2016 *Scientific Reports* **6** 37748
[23] Zhang K, Li H H, Grünberg P, Li Q, Ye S T, Tian Y F, Yan S S, Lin Z J, Kang S S, Chen Y X, Liu G L and Mei L M 2015 *Scientific Reports* **5** 14249
[24] Cheng B, Qin H W and Hu J F 2017 *J. Phys. D: Appl. Phys.* **50** 445001
[25] Guillet T, Zucchetti C, Barbedienne Q, Marty A, Isella G, Cagnon L, Vergnaud C, Jaffrès H, Reyren N, George J M, Fert A and Jamet M 2020 *Phys. Rev. Lett.* **124** 027201
[26] Chen J J, Zhang X Z, Luo Z C, Wang J M and Piao H G 2014 *J. Appl. Phys.* **116** 114511
[27] da Silva A F, Toloza Sandoval M A, Levine A, Levinson E, Boudinov H and Sernelius B E 2020 *J. Appl. Phys.* **127** 045705
[28] He X, Yang F L, Niu H Y, Wang L F, Yi L Z, Xu Y L, Liu M, Pan L Q and Xia Z C 2024 *Chin. Phys. B* **33** 037504
[29] Wang T, Yang D Z, Si M S, Wang F C, Zhou S M and Xue D Z 2016 *Adv. Electron. Mater.* **2** 1600174
[30] He X, He B, Yu H, Sun Z G, He J and Zhao W Y 2019 *J. Appl. Phys.* **125** 224502
[31] He X, Sun Z G, Pang Y Y and Li Y C 2017 *J. Appl. Phys.* **121** 114501
[32] Wu L H, Zhang X, Vanacken J, Schildermans N, Wan C H and Moshchalkov V V 2011 *Appl. Phys. Lett.* **98** 112113
[33] Yang D Z, Wang F C, Ren Y, Zuo Y L, Peng Y, Zhou S M and Xue D S 2013 *Advanced Functional Materials* **23** 2918
[34] Wan C H, Zhang X Z, Gao X L, Wang J M and Tan X Y 2011 *Nature* **477** 304
[35] Delmo M P, Yamamoto S, Kasai S, Ono T and Kobayashi K 2009 *Nature* **457** 1112
[36] He X, Nie Z, Huang Z, Cai L, Duan B and Pan L 2025 *Semiconductors* **59** 844
[37] He X and Sun Z G 2018 *Chin. Phys. B* **27** 067204
[38] Sun Z G, Mizuguchi M, Manago T and Akinaga H 2004 *Appl. Phys. Lett.* **85** 5643
[39] Ali M N, Xiong J, Flynn S, Tao J, Gibson Q D, Schoop L M, Liang T, Haldolaarachchige N, Hirschberger M, Ong N P and Cava R J 2014 *Nature* **514** 205
[40] Xu R, Husmann A, Rosenbaum T F, Saboungi M L, Enderby J E and Littlewood P B 1997 *Nature* **390** 57
[41] Wang J M, Zhang X Z, Piao H G, Luo Z C, Xiong C Y, Wang X F and Yang F H 2014 *Appl. Phys. Lett.* **104** 243511
[42] Keldysh L V 1965 *Soviet Physics JETP* **21** 1135
[43] Zhou G, Duan S, Li P, Sun B, Wu B, Yao Y, Yang X, Han J, Wu J, Wang G, Liao L, Lin C, Hu W, Xu C, Liu D, Chen T, Chen L, Zhou A and Song Q 2018 *Adv. Electron. Mater.* **4** 1700567

[44] Delmo M P, Shikoh E, Shinjo T and Shiraishi M 2013 *Phys. Rev. B* **87** 245301
[45] Hirohata T, Suzuki T, Nakajima K and Mizushima Y 1993 *Jpn. J. Appl. Phys.* **32** 3700
[46] Singh R, Luo Z C, Lu Z Y, Saleemi A S, Xiong C Y and Zhang X Z 2017 *Appl. Phys. Lett.* **111** 042406
[47] Velichko A V, Makarovsky O, Mori N, Eaves L, Krier A, Zhuang Q and Patanè A 2014 *Phys. Rev. B* **90** 085309
[48] Lee J, Joo S, Kim T, Kim K H, Rhie K, Hong J and Shin K H 2010 *Appl. Phys. Lett.* **97** 253505
[49] Schoonus J J H M, Haazen P P J, Swagten H J M and Koopmans B 2009 *J. Phys. D: Appl. Phys.* **42** 185011
[50] Estermann I and Foner A 1950 *Phys. Rev.* **79** 365
[51] Wan C H, Yuan Z H, Liu P, Wu H, Guo P, Li D L and Ali S S 2013 *Appl. Phys. Lett.* **103** 262406
[52] Ahmad F R 2015 *Appl. Phys. Lett.* **106** 012109